PROCEEDINGS OF SCIENCE

# Polarization Reconstruction of Askaryan Emission of Ultra-High Energy Neutrinos Using the Askaryan Radio Array

**Justin Flaherty**[a,*] **for the ARA Collaboration**
(a complete list of authors can be found at the end of the proceedings)

[a] *The Ohio State University,*
*281 W Lane Ave, Columbus, OH, United States*

*E-mail:* flaherty.147@osu.edu

The Askaryan Radio Array (ARA) is an ultra-high energy (> 10 PeV) neutrino detector located in the Dark Sector of the South Pole. It consists of five in-ice stations of antennas that are designed to detect radiation emitted by relativistic particle showers that are byproducts of neutrino interactions in the ice, which generate a cone of Cherenkov radiation in the radio regime (known as Askaryan radiation). The neutrino direction can be reconstructed through a combination of the direction of the Askaryan radiation, its polarization, and its frequency content. Since neutrinos are unaffected by electromagnetic forces and virtually unaffected by gravity, they travel in a straight line through the universe. This allows us to point them back towards potential sources. Through the use of radio pulser measurements, which are controlled radio emissions with a known polarization signature, we can evaluate our reconstruction techniques. Here I will show our reconstruction resolution after applying our reconstruction methods to pulser measurements.

The 38th International Cosmic Ray Conference (ICRC2023)
26 July – 3 August, 2023
Nagoya, Japan

*Speaker





PoS(ICRC2023)1164

## 1. Introduction

Neutrinos are a useful tool for probing the universe, as they are unaffected by electromagnetism and virtually unaffected by gravity. It has been discovered that when an ultra-high energy (UHE) neutrino interacts in a dense dielectric medium, it induces a particle shower and emit coherent Cherenkov radiation in the radio regime [1, 2]. Detecting the radio emission via the Askaryan effect offers a unique opportunity to study these ultra-high energy neutrinos. The Askaryan Radio Array (ARA) is located beneath the ice at the South Pole (see Figure 1), and is designed to detect the radio signal created by UHE neutrinos above 10 PeV. Understanding the polarization properties of the Askaryan emission will enhance our understanding of neutrino interactions in the South Pole ice, as well as the ice itself which exhibits birefringent properties [3, 4].

This paper aims to explore methodologies in reconstructing the polarization of simulated radio pulsers as measured by Station A2 and the reconstruction resolution as a result of those methods. This work serves as a continuation of a past exploration into this topic that sought to reconstruct the polarization [5]. A key difference in this current effort is a change in the geometry defining the polarization, which is laid out in Section 2.1. There are a few things we wish to note about this analysis:

- The results in this paper are only for simulated pulser measurements. We plan on expanding this analysis to real data in the near future.
- We have yet to study the systematic uncertainties of our reconstruction, so we only show statistical error.
- In our pulser simulations, the polarization is calculated at the receiver rather than the source. We plan to update our simulations to define the polarization at the source and implement birefringence [3, 4] in the ice to study how the polarization changes as the ray propagates. Additionally, we need to model the response of the transmitting antenna.
- At present, our simulations do not implement the cross-polarization response in our antennas. We plan on implementing that in the future for this analysis.
- We use a channel-by-channel response for our electronics/amplification, but our antenna response is simply based on antenna type.

## 2. Methodology

### 2.1 Defining the Polarization

Following convention set in [3] we define the polarization angle as shown in Figure 2, where it is defined as the angle with respect to the vertical ($-\hat{\theta}$-direction) in the $\hat{k}$-plane. This means that a pure vertically polarized (VPol) signal would be at an angle of $\Psi = 0$, while a pure horizontally polarized (HPol) signal would be at an angle of $\Psi = 90°$. By simple geometry, the polarization angle $\Psi$ follow the equation:

$$tan\,(\Psi) = \frac{\hat{p}\cdot\hat{\phi}}{\hat{p}\cdot\hat{\theta}} \tag{1}$$

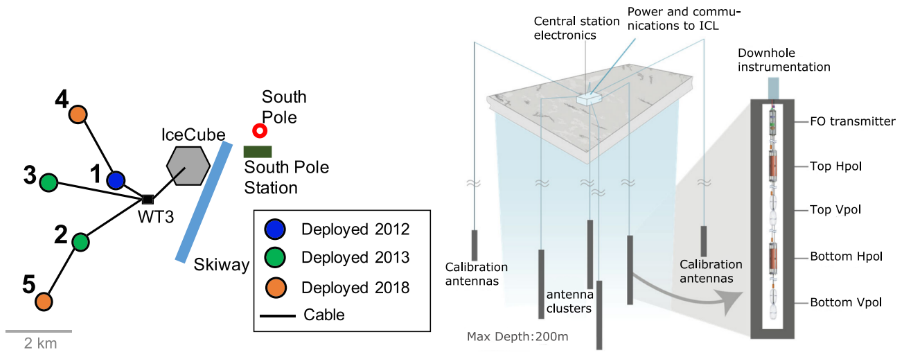


**Figure 1:** (Left) A top-down view of the ARA5 instrument deployed at the South Pole. Station A2 is the focus of the analysis described in this paper. (Right) A schematic of an ARA station showing the arrangement of the VPol and HPol antennas. FO is a fiber-optic transmitter. [6]

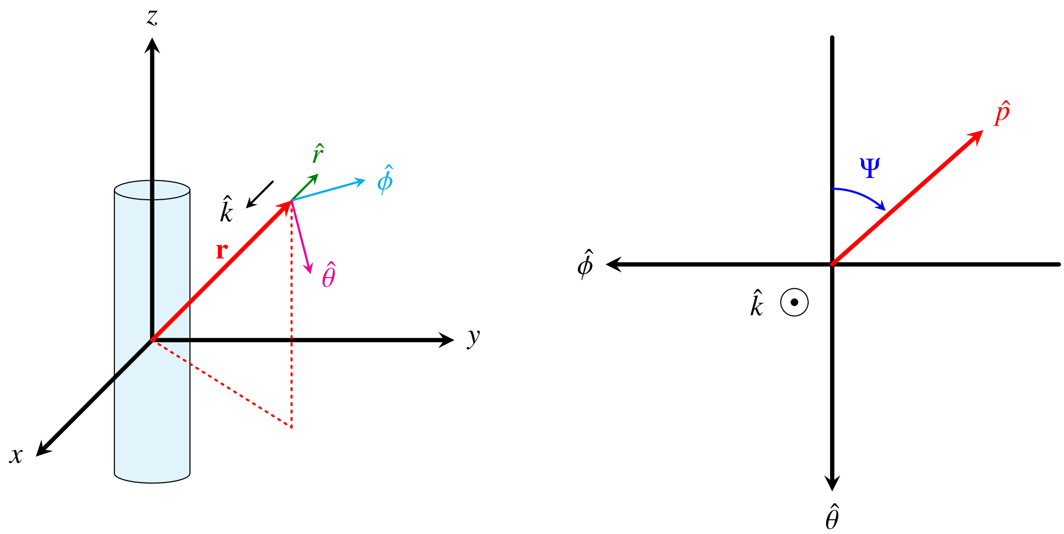


**Figure 2:** Illustration of how we define the polarization angle $\Psi$. For an antenna oriented along the $z$-axis (cyan cylinder) and an incoming RF signal traveling in the $\hat{k}$-direction, the polarization angle is defined with respect to the vertical in the plane of $\hat{k}$. The projections of the polarization vector $\hat{p}$ onto $\hat{\theta}$ and $\hat{\phi}$ are used to calculate the polarization angle $\Psi$ as shown in Equation 1 as well as in the polarization factor defined in Equation 6.

This definition of the polarization is in contrast to past work in [5], where the polarization is defined using angles with respect to the $z$-axis of the antenna. Defining the polarization in $\hat{k}$-plane simplifies the analysis and allows for a more intuitive understanding of the polarization. We do not study the polarity of our signal in this analysis (i.e. what quadrant of the $\hat{k}$-plane $\hat{p}$ points into), so we constrain our analysis for simulated pulses with the domain of $\Psi \in [0, 90°]$.

## 2.2 Simulating Antenna and Electronics Response

We explored the reconstruction of the polarization by simulating a simple pulse given by an IDL (Instrumentation Design Lab) pulser used in Spice Pulser from UNiversity of Kansas (SPUNK), which was lowered into the borehole drilled South Pole Ice Core Experiment (SPICE) [7]. We accomplished this by crafting simulations where Station A2 would detect RF pulses at the SPICE borehole ~2.3 kilometers away with the pulser one kilometer below the surface of the ice. We use AraSim [8], which simulates the ice attenuation, antenna response, and frequency response. It does not yet have the capability to simulate cross-pol response, which we plan on implementing into AraSim and this analysis in the future.

When the signal reaches the detector, AraSim applies the antenna and electronics response as follows. Let $\mathbf{E}(t)$ be the electric field of the signal at the detector. The time-dependent voltage measured by the antenna is given by the projection of the electric field onto the effective height $h_{\text{eff}}$ of the antenna.

$$V(t) \propto \mathbf{h}_{\text{eff}} \cdot \mathbf{E}(t) \tag{2}$$

There are additional steps to incorporate the gain of our antenna and electronics/amplifier, which we lay out below. To simplify our calculations, separate our electric field into its time-dependent ampltitude $E(t)$ and the direction of its polarization $\hat{p}$. We then transform it into the frequency domain

$$E(t) \longrightarrow \tilde{E}(\omega) = |\tilde{E}(\omega)| \cdot e^{i\Phi_0} \tag{3}$$

where $\Phi_0$ is the initial phase of the signal. The electronics and antenna response is given by the transfer function below.

$$G_{\text{elec}}(\omega, ch) = g_{\text{elec}}(\omega, ch) \cdot e^{-i\Phi_{\text{elec}}(\omega, ch)} \tag{4}$$

$$G_{\text{ant}}\left(\omega, \hat{k}, \hat{p}, j\right) = \frac{1}{2\sqrt{2}} h_{\text{eff}}\left(\omega, \hat{k}, j\right) \cdot P(\hat{p}, j) \cdot e^{i\Phi_{\text{ant}}(\omega, \hat{k}, j)} \tag{5}$$

$$P(\hat{p}, j) = \begin{cases} \hat{p} \cdot \hat{\theta} & \text{if } j = 0 \\ \hat{p} \cdot \hat{\phi} & \text{if } j = 1 \end{cases} \tag{6}$$

Where $\omega$ is the frequency of the measured radio signal, $ch$ is the channel of our station, $\hat{k}$ is the trajectory of the incoming radio signal, $h_{\text{eff}}$ is the effective height of our measuring antenna (which contains the antenna gain), $g_{\text{elec}}$ is the electronics gain, $P$ is our polarization factor (projection of electric field onto the antenna), $j$ indicates if the signal was measured by a VPol ($j = 0$) or HPol ($j = 1$) antenna, and $\Phi$ are the phase terms. The gain, effective height, and phase terms are data-driven models that are packaged into AraSim [8], which are on a per-channel basis for the electronics response but only a per-antenna-type basis for the antenna response. The $\frac{1}{\sqrt{2}}$ term in Equation 5 is due to a 3 dB splitter in the ARA Data Acquisition System [9], whereas the $\frac{1}{2}$ term is for calculating power from the effective height [10]. The transfer functions are then applied to the original waveform in the frequency domain, then converted back to the time domain.

$$\tilde{V}(\omega) = G_{\text{elec}} * G_{\text{ant}} * \tilde{E}(\omega) \longrightarrow V(t) \tag{7}$$

Where $V(t)$ is the time-dependent voltage measured at the receiver. Our goal is to deconvolve those waveforms in order to extract the polarization factor $P$ defined in Equation 6, so that we may calculate the polarization angle.

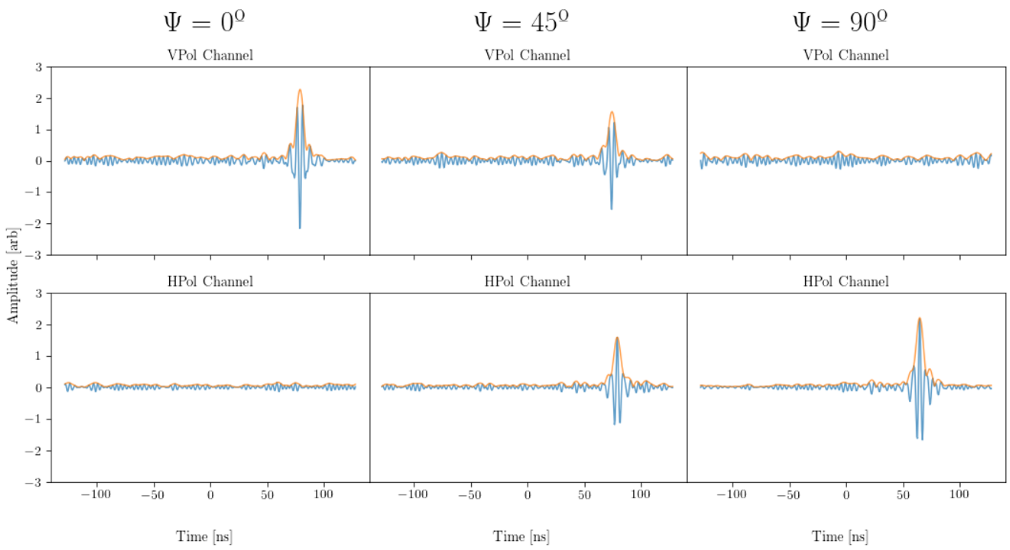


**Figure 3:** Examples of simulated waveforms (measured voltage versus time) at different polarization angles $\Psi$ as measured by the A2 station with our deconvolution applied as described in Section 2.3. The top row are the measurements in the VPol channel, while the bottom represents the HPol channel. The orange trace represents the Hilbert envelope, which we use to find our peak ampltitude. Note that in channels where we expect no signal (HPol for $\Psi = 0$ and VPol for $\Psi = 90$) we measure noise that we cannot fully eliminate, which causes an offset in our reconstruction as seen in Figure 5.

We calculate the signal-to-noise ratio (SNR) of our waveform using the time-dependent voltage in Equation 7 for the VPol and HPol channels following convention in [5] and given by the equation below:

$$\mathrm{SNR} = \frac{\mathrm{V_{peak}}}{\sigma_{\mathrm{noise}}} \tag{8}$$

where $V_{\mathrm{peak}}$ is the absolute value of the peak amplitude across the waveform, and $\sigma_{\mathrm{noise}}$ is the root-mean-square of the noise obtained from the first 50 ns of the waveform. The SNR for different expected polarization angles $\Psi$ are shown in Figure 4, where the VPol (HPol) SNR is defined as the median SNR across VPol (HPol) channels for a single event.

### 2.3 Deconvolving the Waveform

To reconstruct the polarization, we must reconstruct the location of the source using a standard ARA source reconstruction algorithm. This source reconstruction is not the focus of this paper, but is described in detail in [6, 7, 11, 12]. It calculates the location of the source, then calculates the appropriate $\hat{k}$ for each antenna using a depth-dependent index of refraction described by

$$n\,(z) = n_d - (n_d - n_s)\,e^{n_c \cdot z} \tag{9}$$

for negative depths $z$ below the surface of the ice, and where $n_s = 1.35$, $n_d = 1.78$, and $n_c = 0.0132\,m^{-1}$ are generated from a fit of index of refraction versus depth in [13]. Due to the varying index of refraction with ice, the radio pulses will follow an arc between the source and receiver. This allows for two ray-tracing solutions: a direct ray and a refracted/reflected ray [7]. For this analysis, we focus only on the direct ray solutions.

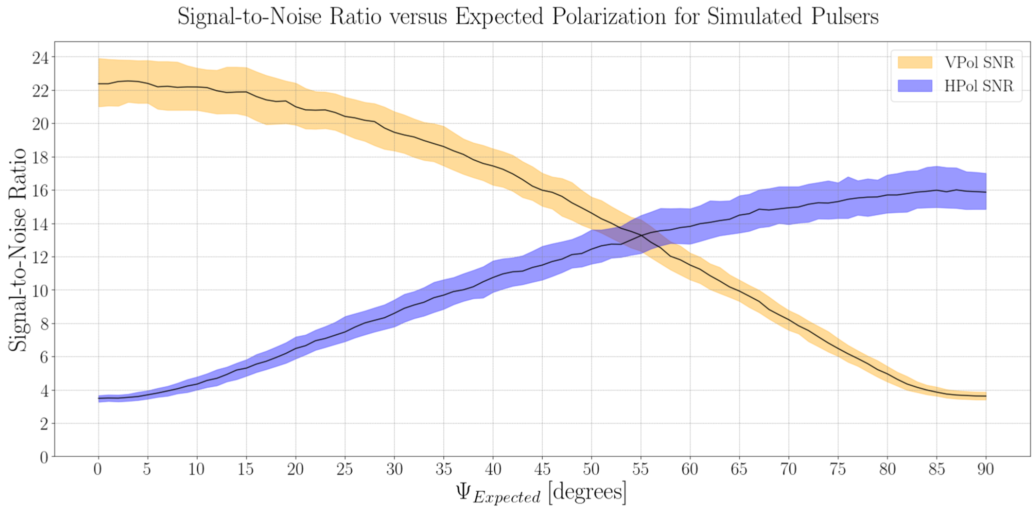


**Figure 4:** Signal-to-noise ratio (SNR) prior to deconvolution for VPol and HPol versus expected polarization for the simulated IDL pulser at 1000 meters in depth located at the SPICE borehole. We find that for strong VPol signals ($\Psi$ near zero) our HPol SNR is low. Similarly, for strong HPol signals ($\Psi$ near 90 degrees) our VPol SNR is low. In these low signal regions, our noise fluctuations are large enough to exceed the RMS noise $\sigma_{\text{noise}}$ defined in Equation 8, causing a $V_{\text{peak}} > \sigma_{\text{noise}}$, which gives a SNR $> 1$. This causes an offset in our reconstructed $\Psi$ near zero and 90°, which we see in Figure 5. Additionally, due to our VPol and HPol antenna having different effective heights, the SNR of a pure HPol signal ($\Psi = 90°$) in an HPol channel will always be lower than that of a pure VPol signal ($\Psi = 0°$) in a VPol channel, which is the reason for the blue HPol curve not reaching the lower maximum SNR compared to the yellow VPol curve; as well as the reason for the two curves crossing at $\Psi_{\text{Expected}} = 55°$ rather than 45°.

We convert our measured waveform into the frequency domain and apply a Butterworth bandpass filter from 150 MHz to 300 MHz to reduce out-of-band noise, as we expect the pulser signal to be strongest in the aforementioned range. We then calculate the entire electronics response in Equation 4 as well as the antenna phase and effective height terms in Equation 5. With those values, we can define transfer functions that invert our antenna and electronics terms:

$$G_{\text{elec}}^{-1}(\omega, ch) = (g_{\text{elec}}(\omega, ch))^{-1} \cdot e^{i\Phi_{\text{elec}}(\omega, ch)} \tag{10}$$

$$G_{\text{ant}}^{*-1}\left(\omega, \hat{k}, \hat{p}, j\right) = \left(\frac{1}{2\sqrt{2}} h_{\text{eff}}\left(\omega, \hat{k}, j\right)\right)^{-1} \cdot e^{-i\Phi_{\text{ant}}(\omega, \hat{k}, j)} \tag{11}$$

Where Equation 11 isn't the exact inverse of Equation 5, as we do not know the polarization of our signal at this stage of the analysis, so we cannot invert the polarization factor $P$. If we apply these inverse functions on our measured waveform, we are left with a deconvolved waveform that still has the polarization factor folded into it.

$$\tilde{V}_D(\omega) = G_{\text{ant}}^{*-1} * G_{\text{elec}}^{-1} * \tilde{V}(\omega) = P(\hat{p}, j) * \tilde{E}(\omega) \tag{12}$$

Where $V_D$ is our deconvolved signal. The polarization factor is a scalar and is independent of frequency, so it is unaffected by Fourier Transforms and allows us to write our deconvolved waveform in the time-domain as:

$$V_D\left(t\right) = P\left(\hat{p}, j\right) \cdot E\left(t\right) \tag{13}$$

The term $E(t)$ represents the electric field of our signal when it arrives at our antenna. The A2 station (as well as other ARA stations) are designed such that each string has a top and bottom pair of VPol and HPol antenna (see Figure 1), where the components of each pair are separated by three meters. It is then assumed that the component antennas of each pair measure the VPol and HPol components of the same electric field. We can then assume, for partner VPol and HPol pairs, that the amplitude $E(t)$ is equal across both antennas. Thus if we take the ratio of measured signal $V_D(t)$ and utilize Equation 1 we would find the polarization angle $\Psi$.

$$\frac{V_{D,\mathrm{HPol}}}{V_{D,\mathrm{VPol}}} = \frac{P\left(\hat{p}, j=1\right) \cdot E\left(t\right)}{P\left(\hat{p}, j=0\right) \cdot E\left(t\right)} = \frac{\hat{p} \cdot \hat{\phi}}{\hat{p} \cdot \hat{\theta}} = tan\left(\Psi\right) \tag{14}$$

In our analysis, we calculate the Hilbert envelope of our deconvolved signal (as shown in Figure 3 and find the time-stamp of the larger peak amplitude between partner HPol and VPol channels. In Figure 3 the VPol signal is clearly larger for the $\Psi = 0$ case, we then use a $20\,ns$ window centered around the time stamp of that peak to find the amplitude in the HPol channel. The $20\,ns$ is to account for differences in arrival time at the antenna. We excluded channel pairs 5/13 and 7/15 to match our on-going analysis of real SPIceCore pulser data. Channel 5/13 is removed due to the direct pulse getting cut off in the beginning of the waveform, whereas Channel 7/15 is removed due to anomalous behavior in the HPol amplification. We then take the ratio of Hilbert peaks at those time-stamps to minimize the effect of noise and obtain our polarization angle.

## 3. Results and Conclusions

The goal of this paper is to show our current efforts on reconstructing the polarization of simulated radio pulsers using the ARA Station A2. Following the steps laid out in Section 2.3, we performed our reconstruction in the absence of systematic uncertainties and cross-polarization response and show our reconstruction resolution in Figure 5. This resolution was calculated by averaging over six of the eight VPol/HPol antenna pairs in A2. The offsets in our reconstruction near $\Psi = 0$ and $\Psi = 90°$ are due to low signal-to-noise ratio in the HPol and VPol channels, respectively, as shown in Figure 4. We expect that this offset can be decreased by a reduction of the in-band noise and signals with higher signal-to-noise ratio.

As we have previously noted, our simulations are not yet capable of simulating cross-polarization and we do not consider systematic uncertainties in our reconstruction. Previous results in [5] quoted a resolution of approximately 5° whereas we quote less $< 1°$ due to using a simplified coordinate system described in [3] and shown in Figure 2, and averaging over six quality channel pairs. Compared to previous work, this is based on simulated pulsers rather than neutrinos, and channel-to-channel variations in amplification gains are also included. Both of these resolutions are at a signal-to-noise ratio of approximately 20 in ARA's system, which correspond to a signal-to-noise ratio of approximately 5 in [14] where a resolution of 2.7° was quoted using SPICE data. In on-going work, we will implement antenna cross-polarization and systematic uncertainties, including channel-to-channel variations in antenna gain, which we expect to affect the accuracy but not the precision quoted here.



PoS(ICRC2023)1164

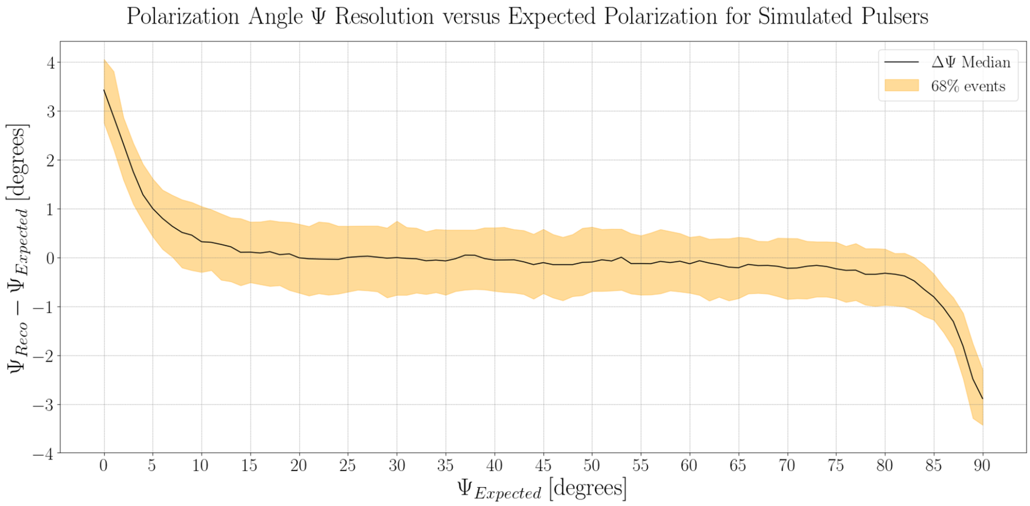


**Figure 5:** Resolution versus expected polarization angle, averaged across VPol/HPol channel pairs, for a simulated IDL pulser at 1000 meters in depth at the SPICE borehole. We simulated 100 events at each $\Psi_{\text{Expected}} \in [0, 90°]$ in increments of 1° for a total of 9100 events. The orange band represents the 68% containment of events, but we wish to note that it only shows the statistical error. Our next step is to consider the systematic uncertainties. The offset in median near $\Psi_{\text{Expected}} = 0$ is due to noise overpowering the weak HPol signal and similarly for weak VPol signal in the $\Psi_{\text{Expected}} = 90°$ region. This median can be brought closer to zero in those regions with further noise reduction and pulses with a higher signal-to-noise ratio.

## References

[1] G. A. Askar'yan *Zh. Eksp. Teor. Fiz.* **41** (1961) 616–618.

[2] D. Saltzberg *et al.* *Phys. Rev. Lett.* **86** (Mar, 2001) 2802–2805.

[3] A. Connolly *Phys. Rev. D* **105** (Jun, 2022) 123012.

[4] T. M. Jordan *et al.* *Annals of Glaciology* **61** no. 81, (2020) 84–91.

[5] J. Torres, *Neutrino Astrophysics with the Askaryan Radio Array*. PhD thesis, The Ohio State University, 2021.

[6] **ARA** Collaboration, P. Allison *et al.* *Phys. Rev. D* **102** (Aug, 2020) 043021.

[7] **ARA** Collaboration, P. Allison *et al.* *Journal of Cosmology and Astroparticle Physics* **2020** no. 12, (Dec, 2020) 009.

[8] **ARA** Collaboration, P. Allison *et al.* *Astroparticle Physics* **70** (2015) 62–80.

[9] **ARA** Collaboration, P. Allison *et al.* *Astroparticle Physics* **35** no. 7, (Feb., 2012) 457–477.

[10] J. D. Kraus, *Antennas*. McGraw-Hill, 1988.

[11] **ARA** Collaboration, P. Allison and others. *Phys. Rev. D* **105** (Jun, 2022) 122006.

[12] B. Clark, *Optimization of a Search for Ultra-High Energy Neutrinos in Four Years of Data of ARA Station 2*. PhD thesis, The Ohio State University, 2019.

[13] I. Kravchenko, D. Besson, and J. Meyers *Journal of Glaciology* **50** no. 171, (2004) 522–532.

[14] **ARIANNA** Collaboration, A. Anker *et al.* *Journal of Instrumentation* **15** no. 09, (Sep, 2020) P09039.

## Full Author List: ARA Collaboration (July 14, 2023)

S. Ali[1], P. Allison[2], S. Archambault[3], J.J. Beatty[2], D.Z. Besson[1], A. Bishop[4], P. Chen[5], Y.C. Chen[5], B.A. Clark[6], W. Clay[7], A. Connolly[2], K. Couberly[1], L. Cremonesi[8], A. Cummings[9,10,11], P. Dasgupta[12], R. Debolt[2], S. de Kockere[13], K.D. de Vries[13], C. Deaconu[7], M. A. DuVernois[4], J. Flaherty[2], E. Friedman[6], R. Gaior[3], P. Giri[14], J. Hanson[15], N. Harty[16], B. Hendricks[9,10], K.D. Hoffman[6], J.J. Huang[5], M.-H. Huang[5,17], K. Hughes[9,10,11], A. Ishihara[3], A. Karle[4], J.L. Kelley[4], K.-C. Kim[6], M.-C. Kim[3], I. Kravchenko[14], R. Krebs[9,10], C.Y. Kuo[5], K. Kurusu[3], U.A. Latif[13], C.H. Liu[14], T.C. Liu[5,18], K. Mase[3], M.S. Muzio[9,10,11], J. Nam[5], R.J. Nichol[8], A. Novikov[16], A. Nozdrina[1], E. Oberla[7], Y. Pan[16], C. Pfendner[19], N. Punsuebsay[16], J. Roth[16], A. Salcedo-Gomez[2], D. Seckel[16], M.F.H. Seikh[1], Y.-S. Shiao[5,20], D. Smith[7], S. Toscano[12], J. Torres[2], J. Touart[6], N. van Eijndhoven[13], G.S. Varner[21], A. Vieregg[7], M.-Z. Wang[5], S.-H. Wang[5], S.A. Wissel[9,10,11], C. Xie[8], S. Yoshida[3], R. Young[1]

[1] Dept. of Physics and Astronomy, University of Kansas, Lawrence, KS 66045
[2] Dept. of Physics, Center for Cosmology and AstroParticle Physics, The Ohio State University, Columbus, OH 43210
[3] Dept. of Physics, Chiba University, Chiba, Japan
[4] Dept. of Physics, University of Wisconsin-Madison, Madison, WI 53706
[5] Dept. of Physics, Grad. Inst. of Astrophys., Leung Center for Cosmology and Particle Astrophysics, National Taiwan University, Taipei, Taiwan
[6] Dept. of Physics, University of Maryland, College Park, MD 20742
[7] Dept. of Physics, Enrico Fermi Institue, Kavli Institute for Cosmological Physics, University of Chicago, Chicago, IL 60637
[8] Dept. of Physics and Astronomy, University College London, London, United Kingdom
[9] Center for Multi-Messenger Astrophysics, Institute for Gravitation and the Cosmos, Pennsylvania State University, University Park, PA 16802
[10] Dept. of Physics, Pennsylvania State University, University Park, PA 16802
[11] Dept. of Astronomy and Astrophysics, Pennsylvania State University, University Park, PA 16802
[12] Université Libre de Bruxelles, Science Faculty CP230, B-1050 Brussels, Belgium
[13] Vrije Universiteit Brussel, Brussels, Belgium
[14] Dept. of Physics and Astronomy, University of Nebraska, Lincoln, Nebraska 68588
[15] Dept. Physics and Astronomy, Whittier College, Whittier, CA 90602
[16] Dept. of Physics, University of Delaware, Newark, DE 19716
[17] Dept. of Energy Engineering, National United University, Miaoli, Taiwan
[18] Dept. of Applied Physics, National Pingtung University, Pingtung City, Pingtung County 900393, Taiwan
[19] Dept. of Physics and Astronomy, Denison University, Granville, Ohio 43023
[20] National Nano Device Laboratories, Hsinchu 300, Taiwan
[21] Dept. of Physics and Astronomy, University of Hawaii, Manoa, HI 96822

**Acknowledgements**

The ARA Collaboration is grateful to support from the National Science Foundation through Award 2013134. The ARA Collaboration designed, constructed, and now operates the ARA detectors. We would like to thank IceCube and specifically the winterovers for the support in operating the detector. Data processing and calibration, Monte Carlo simulations of the detector and of theoretical models and data analyses were performed by a large number of collaboration members, who also discussed and approved the scientific results presented here. We are thankful to the Raytheon Polar Services Corporation, Lockheed Martin, and the Antarctic Support Contractor for field support and enabling our work on the harshest continent. We are thankful to the National Science Foundation (NSF) Office of Polar Programs and Physics Division for funding support. We further thank the Taiwan National Science Councils Vanguard Program NSC 92-2628-M-002-09 and the Belgian F.R.S.- FNRS Grant 4.4508.01 and FWO. K. Hughes thanks the NSF for support through the Graduate Research Fellowship Program Award DGE-1746045. B. A. Clark thanks the NSF for support through the Astronomy and Astrophysics Postdoctoral Fellowship under Award 1903885, as well as the Institute for Cyber-Enabled Research at Michigan State University. A. Connolly thanks the NSF for Award 1806923 and 2209588, and also acknowledges the Ohio Supercomputer Center. S. A. Wissel thanks the NSF for support through CAREER Award 2033500. A. Vieregg thanks the Sloan Foundation and the Research Corporation for Science Advancement, the Research Computing Center and the Kavli Institute for Cosmological Physics at the University of Chicago for the resources they provided. R. Nichol thanks the Leverhulme Trust for their support. K.D. de Vries is supported by European Research Council under the European Unions Horizon research and innovation program (grant agreement 763 No 805486). D. Besson, I. Kravchenko, and D. Seckel thank the NSF for support through the IceCube EPSCoR Initiative (Award ID 2019597). M.S. Muzio thanks the NSF for support through the MPS-ASCEND Postdoctoral Fellowship under Award 2138121.